Magnetic field dependence of the basal-plane superconducting anisotropy in $YBa_2Cu_4O_8$ from small-angle neutron scattering measurements of the vortex lattice

Jonathan S. White,[1,2,3,*] Charlotte J. Bowell,[2] Alistair S. Cameron,[2] Richard W. Heslop,[2] Joël Mesot,[1,3,4] Jorge L. Gavilano,[1] Simon Strässle,[5] Lars Mächler,[1] Rustem Khasanov,[6] Charles D. Dewhurst,[7] Janusz Karpinski,[4] and Edward M. Forgan[2]

[1]*Laboratory for Neutron Scattering, Paul Scherrer Institut, CH-5232 Villigen, Switzerland*
[2]*School of Physics and Astronomy, University of Birmingham, Edgbaston, Birmingham, B15 2TT, United Kingdom*
[3]*Institute of Condensed Matter Physics, Ecole Polytechnique Fédérale de Lausanne, CH-1015 Lausanne, Switzerland*
[4]*Laboratory for Solid State Physics, ETH Zürich, CH-8093 Zürich, Switzerland*
[5]*Physik-Institut der Universität Zürich, Winterthurerstrasse 190, CH-8057 Zürich, Switzerland*
[6]*Laboratory for Muon Spin Spectroscopy, Paul Scherrer Institute, CH-5232 Villigen, Switzerland*
[7]*Institut Laue-Langevin, 6 rue Jules Horowitz, 38042 Grenoble, France*

(Received 8 October 2013; revised manuscript received 11 December 2013; published 2 January 2014)

We report a study of the basal-plane anisotropy of the superfluid density in underdoped $YBa_2Cu_4O_8$ (Y124), showing the effects of both the CuO_2 planes and the fully occupied CuO chains. From small-angle neutron scattering measurements of the vortex lattice, we can infer the superconducting (SC) properties for a temperature (T) range $T = 1.5$ K to T_c and magnetic induction B from 0.1 to 6 T. We find that the superfluid density along **a** has a simple d-wave T dependence. However, along **b** (the chain direction) the superfluid density falls much more rapidly with T and also with increasing field. This strongly suggests the suppression of proximity-effect-induced superconductivity in the CuO chains. In addition, our results do not support a common framework for the low-field in-plane SC response in Y124 and related $YBa_2Cu_3O_7$, and also indicate that any magnetic field induced charge-density-wave order in Y124 exists only for fields above 6 T.

DOI: 10.1103/PhysRevB.89.024501 PACS number(s): 74.25.Uv, 61.05.fg, 74.25.Ha, 74.72.−h

I. INTRODUCTION

The unifying structural constituent of all cuprate superconductors is the two-dimensional (2D) CuO_2 planes. The YBaCuO family, $YBa_2Cu_3O_{7-\delta}$ (Y123) and $YBa_2Cu_4O_8$ (Y124), are special since they also host one-dimensional (1D) CuO chains along the crystal **b** axis. For structurally well-ordered chains, the associated electronic states contribute to the Fermi surface. This makes YBaCuO a model system for studying low-dimensional conductors in close proximity. Indeed, it has long been proposed that by proximity to the CuO_2 planes, the CuO chain states become superconducting (SC) below T_c.[1,2] This is supported by the experimentally observed ab-plane SC anisotropy where the London penetration depth is shorter for currents flowing along the **b** axis than the **a** axis. Moreover, the observed anisotropy is larger in Y124,[3,4] which displays two CuO chains per unit cell, than in single-chained Y123.

While proximity-effect (PE) models provide an explanation for the in-plane SC anisotropy, a single framework for both Y123 and Y124 is not supported by experimental evidence. In Y123, a clear electronic anisotropy in the CuO_2 plane reported from transport[5] and ARPES (Ref. 6) studies implies SC chain states are not required to explain the SC anisotropy. Measurements of the London penetration depth λ give further information since for a crystal axis i, $n_i(T) \propto \lambda_i^{-2}(T)$. In Y123, these show that the superfluid density n along both **a** and **b** axes has a d-wave temperature (T) dependence,[7–9] which disagrees with the expectations of PE models.[1,10]

For Y124, the picture is somewhat unclear. It has been suggested that a positive low-T curvature of both $n_a(T)$ and $n_b(T)$ observed by low-field μSR is evidence for a two-gap SC state in the CuO_2 plane.[11] However, from other penetration depth measurements, only $n_b(T)$ was observed to display a positive curvature, while $n_a(T)$ displayed d-wave behavior.[12] These results were argued as evidence for PE-induced SC chain states in Y124.

Here, we present small-angle neutron scattering (SANS) measurements of the vortex lattice (VL) in Y124. Our measurements are conducted over a wide range of magnetic fields and temperatures, and the results cast important light on the plane-chain interplay in YBaCuO compounds. SANS experiments are a bulk probe of both the VL structure and the microscopic field distribution, each of which depend on the SC length scales. Our single-crystal samples of Y124 are naturally twin free, and the stoichiometric oxygen content makes the CuO chains effectively infinite in length. These properties suppress the vortex pinning effects seen in some Y123 samples, such as those due to twin planes and oxygen vacancies.[13–15] Therefore, the results of this study on Y124 provide valuable comparison to the intrinsic VL properties only recently observed in twin-free and fully-oxygenated $YBa_2Cu_3O_7$ (Y1237).[9,16]

As will be seen in what follows, the VL in Y124 displays remarkably different properties to those observed in Y1237. This is apparent from measurements of both the VL structure presented in Sec. III A, and the magnetic field and T dependence of the VL form factor presented in Sec. III B. In Sec. IV, we discuss the new insights provided by our results in connection with important topics relevant for both Y123 and Y124, such as proximity-effect-induced CuO chain superconductivity, the basal-plane superconducting anisotropy, and charge-density-wave order. Finally, a summary is presented in Sec. V. In Sec. II, we begin by detailing the experimental method.

 ©2014 American Physical Society

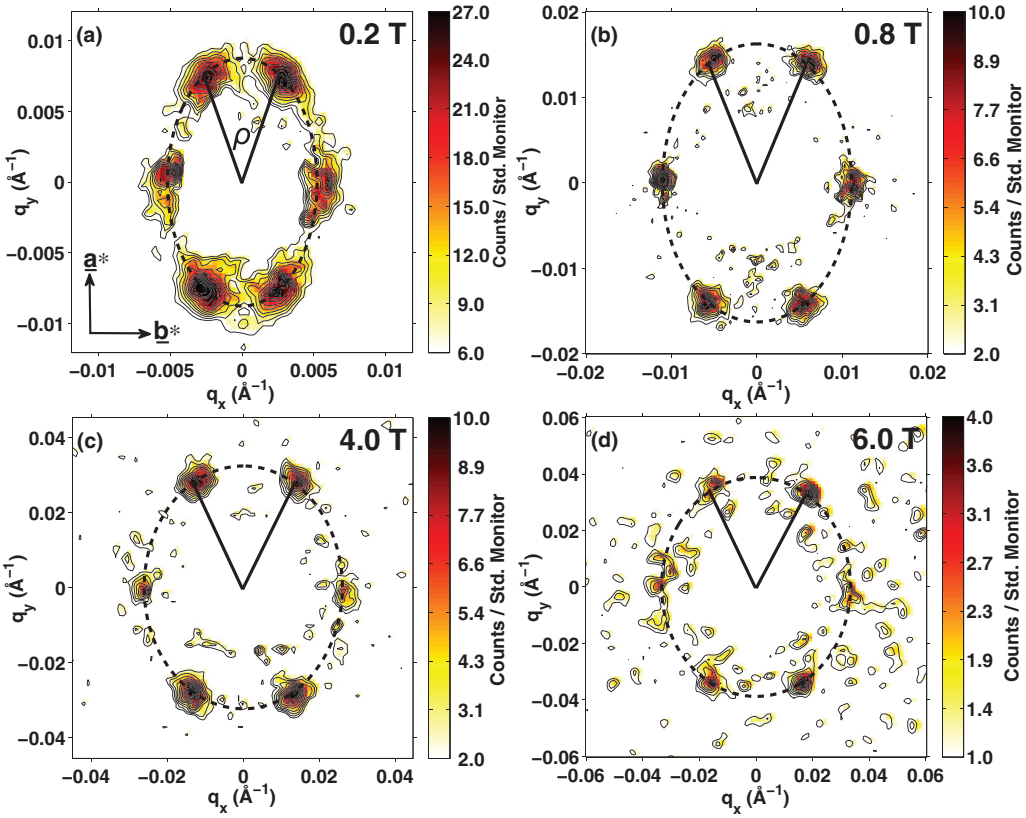

FIG. 1. (Color online) VL diffraction patterns obtained in Y124 at 1.5 K, and in $\mu_0 H \parallel \mathbf{c}$ of (a) 0.2 T, (b) 0.8 T, (c) 4.0 T, and (d) 6.0 T. Each image is the sum of scattering from the VL as the sample is both tilted and rotated so that the Bragg condition is satisfied at the detector for the different diffraction spots. In each image, solid lines show the reciprocal VL basis vectors, and dashed line ellipses emphasize the VL anisotropy. The VL opening angle ρ is defined in (a).

II. EXPERIMENTAL METHOD

Single crystals of $YBa_2Cu_4O_8$ were prepared as described in Ref. 17. Each had approximate size $0.8 \times 0.3 \times 0.05$ mm^3, and the longest side parallel to the **b** axis. To obtain a sample mass suitable for neutron scattering experiments, 130 single crystals of total volume of 3.95×10^{-5} m^2 were mounted onto a thin aluminum plate, each with their **c** axis perpendicular to the plate, and **a** axis vertical. The resulting mosaic had $T_c \simeq 79.9$ K with $\Delta T_c \simeq 2$ K.

The SANS experiments were conducted at the Institut Laue-Langevin, Grenoble, France, and the Swiss spallation neutron source (SINQ), Paul Scherrer Institut, Villigen, Switzerland. The sample mosaic was installed inside either a 6- or 11- T horizontal field cryomagnet that provided a base temperature (T) of 1.5 K. The crystal **c** axis was parallel to the applied magnetic field ($\mu_0 H$), with both approximately parallel to the incident neutron beam. Cold neutrons [$\lambda_n = 0.6$ to 1.66 nm, with full width at half maximum (FWHM) spread of 10%] were collimated over 8–14 m, and after diffracting from the sample, were counted on a position-sensitive multidetector placed 8–14 m away. Measurements carried out at $T > T_c$ were subtracted from those done at low T, in order to leave just the VL signal.

Due to the intrinsically twin-free and stoichiometric properties of the crystals, VL pinning is expected to be suppressed in our sample. Nonetheless, weak pinning due to residual crystal defects may still be expected. In these circumstances, cooling through T_c in a magnetic field that is weakly oscillating around the target field allows the vortices to overcome the pinning potential and attain a coordination closer to equilibrium. Therefore, all measurements reported here were conducted on VLs prepared using a weakly oscillatory magnetic field component of $\pm$0.02–0.05 T during either cooling or warming to the target T. When at the intended T, the field was held stationary at the target value when conducting the SANS measurements.

III. RESULTS

A. Vortex lattice structure

Figure 1 shows VL diffraction patterns obtained from Y124 at T=1.5 K, and over the observable field range up to $\mu_0 H \parallel \mathbf{c} = 6.0$ T. At all fields, the VL forms a single distorted hexagonal domain aligned with the crystal axes. We quantify the distortion in terms of the axial ratio of the ellipse that overlays the Bragg spots η which is related to the VL opening angle ρ by $\eta = [\sqrt{3}\tan(\rho/2)]^{-1}$. The field dependencies of both η and ρ at T=1.5 K are shown in Fig. 2. With increasing $\mu_0 H$, η reduces and the VL structure becomes increasingly isotropic. For comparison, in Fig. 2 we include equivalent data for Y1237.[9,16] It is clear that the low-field dependence of η is much stronger in Y124 than in Y1237. At higher

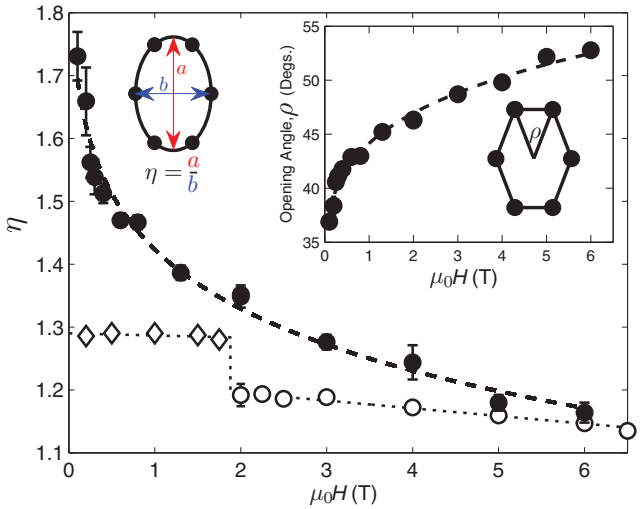

FIG. 2. (Color online) The $\mu_0 H$ dependence of the VL distortion parameter η, defined by the inset sketch. Results for Y124 are shown with filled symbols. Empty symbols denote similar Y1237 data (Refs. 9 and 16). Inset: the $\mu_0 H$ dependence of the VL opening angle ρ in Y124. All lines are guides for the eye.

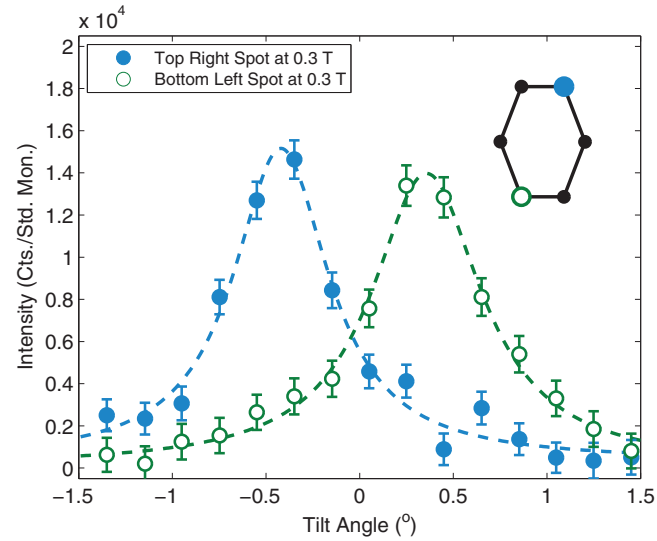

FIG. 3. (Color online) Typical examples of the angular dependence of the diffracted intensity (rocking curves) obtained from the VL in Y124 at $\mu_0 H = 0.3$ T and $T = 1.5$ K. Dashed lines correspond to a fit of a Lorentzian line shape to each curve. The tilt angle corresponds to the rotation angle of the sample and cryomagnet around the horizontal axis. The inset sketch shows the VL structure, with two of the VL spots denoted by symbols that match those of the associated rocking curves.

fields, however, the two compounds display more comparable behavior.

For high-κ materials, and low $\mu_0 H \parallel \mathbf{c}$, anisotropic local London theory[18–20] gives the VL distortion parameter η equal to the in-plane penetration depth anisotropy $\gamma_{ab} = \lambda_a/\lambda_b$. The sign of the observed VL distortion in Y124 shows that $\lambda_a > \lambda_b$, so the supercurrent density is larger along the CuO chain direction. Moreover, η is larger in Y124 than Y1237 for the same fields, thus confirming the more anisotropic SC state in the double-chained compound.[3] For both materials, the $\mu_0 H$-induced suppression of η implies a reduction in γ_{ab} within local theory. However, care must taken if assuming $\eta = \gamma_{ab}$ across the entire T and $\mu_0 H$ ranges. In particular, at high $\mu_0 H$, the equality becomes increasingly invalid due to nonlocal effects.[9] Nonetheless, at low $\mu_0 H$ where local theory is most valid, the two compounds display clearly different behavior. In Y1237, η is constant up to a kink at a VL structure transition at $\sim$2 T, and after that falls monotonically with field.[16] In contrast, η in Y124 varies smoothly over the entire field range, and falls quickly at low fields. These observations show that even close to the local regime, the nonlocal interactions present in each compound lead to markedly different VL properties. In turn, this evidences the very different basal-plane SC responses for Y124 and Y1237.

Since local theory provides no constraint on the VL orientation for $\mu_0 H \parallel \mathbf{c}$, even a weak additional interaction can give a preferred VL alignment. In anisotropic materials such as YBaCuO, this can be due to nonlocal interactions between the VL and the system anisotropies such as those of the Fermi surface[21] and the SC gap.[22,23] Determining which is most influential requires first-principles numerical calculations that include the details of both anisotropies.[24] These calculations will also shed light on why the single VL orientation observed in Y124 is seen only in an intermediate field range 2 T$< \mu_0 H <$ 6.7 T in Y1237.[16] Furthermore, in Y1237 a high-field transition, proposed to be driven by the d-wave gap,[16] separates the intermediate field structure from a rhombic one that evolves smoothly to become almost square by 10.8 T. No sign of a similar transition is observed for $\mu_0 H \leqslant 6.0$ T in our Y124 sample, while for higher fields the SANS VL signal is too weak to observe. To search for a squarelike VL structure in Y124, high-field SANS studies on larger samples are required.

B. Vortex lattice form factor

Next, we discuss measurements of the VL form factor $F(\mathbf{q})$, which is the Fourier transform of the magnetic field modulation in the mixed state. Experimentally, $F(\mathbf{q})$ at the wave vector $\mathbf{q}$ is obtained from the integrated intensity $I_{\mathbf{q}}$ of a VL diffraction spot as it is rotated through the Bragg condition at the detector. Figure 3 shows the typical angular variation of the diffracted intensity (the rocking curve) measured from the low-field VL in Y124. The quantity $I_{\mathbf{q}}$ is obtained by integrating the area underneath the Lorentzian line shape used to fit the curve, and is related to $|F(\mathbf{q})|$ by[25]

$$I_{\mathbf{q}} = 2\pi\phi(\gamma/4)^2 V \lambda_n^2 \Phi_0^{-2} \mathbf{q}^{-1} |F(\mathbf{q})|^2. \quad (1)$$

Here, ϕ is the intensity of the incident neutron beam, γ is the neutron magnetic moment in nuclear magnetons, Φ_0 is the flux quantum, V is the sample volume, and λ_n the neutron wavelength.

1. Field dependence of the form factor

Figure 4(a) shows the $\mu_0 H$ dependence at T=1.5 K of the VL form factor in Y124. In many strongly type-II superconductors, the observed falloff with $\mu_0 H$ can be represented by the anisotropic London model extended by a Gaussian cutoff

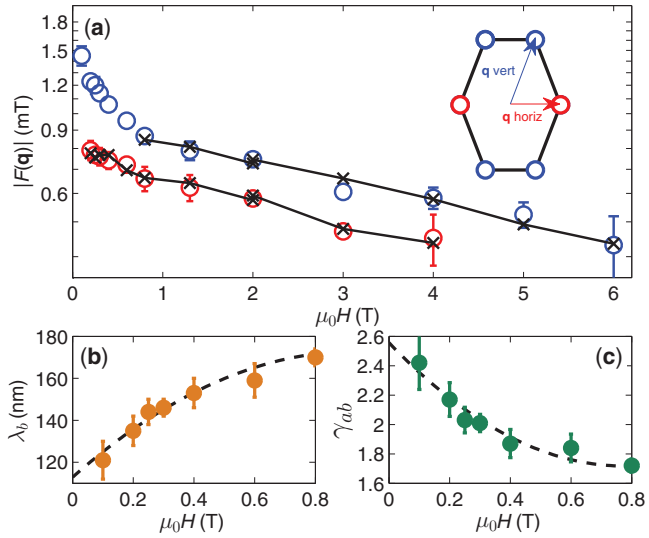

FIG. 4. (Color online) (a) A semilog plot of the $\mu_0 H$ dependence of the VL form factors $|F\,(\mathbf{q}\text{ vert})|$ and $|F\,(\mathbf{q}\text{ horiz})|$ at $T = 1.5$ K. The inset sketch of the VL structure defines the two types of Bragg spot, the form factors of which are treated separately. Black lines are fits of Eq. (2) to the curves using a $\mu_0 H$-independent parameter set (see text for details). Panels (b) and (c), respectively, show the field dependence of λ_b and γ_{ab}, after varying λ_b in Eq. (2) to obtain a good description of the low-field $|F\,(\mathbf{q}\text{ vert})|$ data in (a) (see text for details). Dashed lines are guides for the eye.

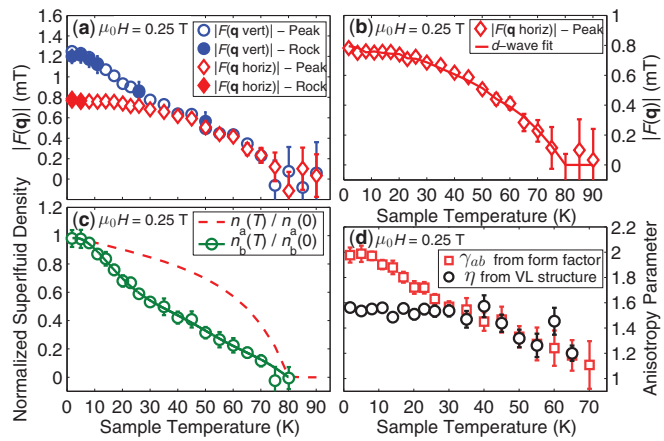

FIG. 5. (Color online) (a) A warming T dependence at $\mu_0 H = 0.25$ T of the VL form factors. Filled and empty symbols, respectively, denote full rocking curve, and rocking-curve peak measurements. (b) The T dependence of $|F\,(\mathbf{q}\text{ horiz})|$. The line is a d-wave model fit to the data with $\Delta_0(0) = 24(2)$ meV. (c) Normalized superfluid densities $n_a(T)$ and $n_b(T)$. The values for $n_b(T)$ are extracted as described in the text. The solid line is a guide to the eye. The dashed line is the ideal curve for $n_a(T)$ obtained from the fit in panel (b). (d) The T dependencies at $\mu_0 H$=0.25 T of the anisotropy parameters γ_{ab} and η.

which represents the finite size of the vortex cores.[9,26,27] The cutoff leads to an expected exponential reduction in $F(\mathbf{q})$ with $\mu_0 H$. The model is valid for both $\kappa \gg 1$ and $H \ll H_{c2}$, and is in general T dependent:

$$F(\mathbf{q},T) = \frac{\langle B\rangle \exp\{-0.44[\mathrm{q}_x^2\xi_b(T)^2 + \mathrm{q}_y^2\xi_a(T)^2]\}}{1 + [\mathrm{q}_x^2\lambda_a(T)^2 + \mathrm{q}_y^2\lambda_b(T)^2]}, \quad (2)$$

where $\langle B\rangle$ is the internal induction. $\xi_i(T)$ and $\lambda_i(T)$, respectively, denote the GL coherence lengths and London penetration depths along directions i. q_x and q_y denote components of $\mathbf{q}$ parallel to $\mathbf{b}^*$ and $\mathbf{a}^*$, respectively. For all fits, we used the experimentally observed $\mathbf{q}$ values.

We note that the horizontal $|F\,(\mathbf{q}\text{ horiz})|$ spots, which have $\mathbf{q} \parallel \mathbf{b}^*$, lie close to a straight line in the semilog plot in Fig. 4(a) and so can be fitted with constant values of just two parameters ξ_b and λ_a in Eq. (2). However, the top/bottom $|F\,(\mathbf{q}\text{ vert})|$ spots have an anomalous behavior for $\mu_0 H < 0.8$ T. Concentrating therefore on fitting just the $|F\,(\mathbf{q}\text{ horiz})|$ spots, we obtain $\xi_b = 3.6(2)$ nm and $\lambda_a = 293(3)$ nm at 1.5 K. The value of ξ_b implies $H_{c2} \sim 25$ T, which is below the recently reported value of 44 T,[28,29] and suggests a contribution of weak VL disorder to the variation of the form factor.[9]

Extending the analysis to the $|F(\mathbf{q}\text{ vert})|$ spots, it is clear that above 0.8 T the model can be applied to fit them too, and we obtain in addition $\lambda_b = 170(4)$ nm and $\xi_a = 3.7(2)$ nm. To capture the behavior of $|F(\mathbf{q}\text{ vert})|$ for $\mu_0 H < 0.8$ T, we first note that according to Eq. (2), ξ_i has little influence at low fields. Therefore, to describe the data, λ_b must become smaller at low field, which corresponds to an increase in the superfluid density for currents along $\mathbf{b}$. Figure 4(b) shows the low $\mu_0 H$ dependence of λ_b which, for all other parameters $\mu_0 H$ independent, gives calculated $|F(\mathbf{q}\text{ vert})|$ values consistent with the experimental data. Using the $\mu_0 H$-dependent values of λ_b, and $\lambda_a = 293(3)$ nm, the low-$\mu_0 H$ dependence of γ_{ab} at 1.5 K is shown in Fig. 4(c).

From our analysis of the $\mu_0 H$-dependent form factor at 1.5 K, there are apparently two disagreements with anisotropic London theory: (a) γ_{ab} is always $>\eta$ at the same field [compare Fig. 4(c) with Fig. 2], and (b) the form factors for the two spot types do not become equal at low fields.[9] Both these discrepancies may arise if the VL structure is T dependent, yet becomes pinned so that the value of η at 1.5 K does not represent the true SC anisotropy, which is γ_{ab}. To demonstrate that this is the case, we consider low-field results at higher T.

2. *Temperature dependence of the form factor*

T-dependent measurements of the VL form factor at low field provide direct insight concerning both the anisotropy of the superfluid density and the underlying gap structure. The intensive nature of these measurements means that there was insufficient neutron beamtime to record full rocking curves, and hence $I_\mathbf{q}$, at each T. Therefore, measurements were done just at the Bragg angle (at the peak of the rocking curve), with full rocking-curve measurements done at selected T's to confirm the T independence of the rocking-curve width. All T-dependent measurements were done by warming scans conducted after an initial oscillation field cool to 1.5 K.

Figure 5(a) shows the T dependence of the form factors at $\mu_0 H = 0.25$ T. We see that on warming, the base-T form factor anisotropy is suppressed, so that the form factors eventually become equal as expected within London theory. To show how both γ_{ab} and η compare at higher T, we will start by obtaining γ_{ab} at each temperature. This is done in two steps. Firstly we need to calculate $\lambda_a(T)$ from the $|F\,(\mathbf{q}\text{ horiz})|$ data, and then subsequently we can extract $\lambda_b(T)$ from the $|F\,(\mathbf{q}\text{ vert})|$

data. For the first step, we see from Eq. (2) that $q_y = 0$ for the $|F(\mathbf{q}\ \text{horiz})|$ spots, and so they are sensitive only to the T variation of $\xi_b(T)$ and $\lambda_a(T)$ from their previously established base-T values. The T variations of both $\xi_b(T)$ and $\lambda_a(T)$ are calculated following the same approach reported in Ref. 9. For calculating $\lambda_a(T)$, we compute the T-dependent quasiparticle spectrum expected over a standard d-wave SC gap on a single quasicylindrical sheet, and for which the zero-T gap magnitude $\Delta_0(T = 0)$ is a free parameter.[30]

In principle, therefore, the fit of the $|F(\mathbf{q}\ \text{horiz})|$ data is dependent on three parameters: $\xi_b(0)$, $\lambda_a(0)$, and $\Delta_0(0)$. We found that the fit was insensitive to $\xi_b(0)$, and so this parameter was fixed at 3.6 nm as determined in Sec. III B 1. As shown in Fig. 5(b), the T dependence of $|F(\mathbf{q}\ \text{horiz})|$ is well described by the d-wave model for the superfluid density, and the two remaining free parameters are fitted to be $\lambda_a = 290(3)$ nm and $\Delta_0(0) = 24(2)$ meV. The good fit and agreement of the parameter values with those reported elsewhere[3,11,31] confirms $n_a(T)$ to be controlled by a single d-wave SC gap.

Next, we extract the T dependence of $n_b(T)$. By using the $|F(\mathbf{q}\ \text{vert})|$ data shown in Fig. 5(a), the d-wave model fit for $n_a(T)$, and the zero-T values for ξ_i obtained in Sec. III B 1, we can solve for the only remaining unknown in Eq. (2), which is $\lambda_b(T)[\propto 1/\sqrt{n_b(T)}]$. The extracted T dependence of $n_b(T)$ is shown in Fig. 5(c). The positive curvature observed below $\sim T_c/2$ is inconsistent with usual d-wave behavior, and instead evidences a multigap SC response along **b**. We also note that the extrapolated value $\lambda_b(0) = 145(2)$ nm at this field agrees with that shown in Fig. 4(b).

Figure 5(d) shows the T dependence of the SC anisotropy parameters at $\mu_0 H = 0.25$ T. Here, γ_{ab} is determined at each T using the absolute $n_i(T)$ data, while η is obtained directly from the VL structure. Above $\sim$30 K, γ_{ab} and η agree well, as expected within anisotropic London theory. For $T < 30$ K, however, a clear difference between γ_{ab} and η emerges, as η varies only weakly on cooling, while γ_{ab} increases smoothly. This behavior, and that of Fig. 5(a), is explained most simply if the VL structure becomes frozen on cooling below $\sim$30 K and is thus unable to evolve further on cooling. Importantly then, the *intrinsic* low-T SC anisotropy is *only* given by γ_{ab} as evaluated using λ_i values obtained from analyzing the form factor. From our T-dependent data, we find that at 0.25 T, $\gamma_{ab} = 1.97(4)$ by 1.5 K, and from data at 0.4 T (see the Appendix A), $\gamma_{ab} = 1.80(2)$. These values agree with those obtained independently from the field-dependent form factor analysis [Fig. 4(c)]. Also, from Fig. 4(c), our extrapolation to zero field of $\gamma_{ab} = 2.57(5)$ agrees well with the value of 2.5 determined by far-infrared spectroscopy.[3]

IV. DISCUSSION

Our analysis of the T-dependent form factor at 0.25 T shows $n_a(T)$ to be mainly sensitive to a single d-wave SC gap of amplitude 24(2) meV, while $n_b(T)$ requires a multigap description. Evidence for a contribution to the multigap response of $n_b(T)$ is provided by ARPES where a $\sim$5-meV gap is observed directly at the crossing point between plane and chain Fermi surfaces.[32] This ties the origin of the gap strongly to plane-chain hybridization as expected within the PE models.[1,10] The field dependence of λ_b at 1.5 K [Fig. 4(c)] likely reflects the quenching of the 5-meV gap, or an as yet unobserved part of the gap structure. We also expect that the sharp change in the $\mu_0 H$ dependence of the form factor ratio observed at $\sim$0.8 T [Fig. 4(a)] marks the field scale of this quenching, such as a critical field of the PE-induced SC response.

Next, we compare the low-$\mu_0 H$ SC responses of Y124 and Y1237. In Y124, the T-dependent forms for both $n_a(T)$ and $n_b(T)$ at $\mu_0 H = 0.25$ T [Fig. 5(c)] are qualitatively similar to those reported at very low field in Ref. 12, and are consistent with a PE model where the plane-chain coupling is mediated via single-electron tunneling.[10] However, this model can not explain low-field SANS data collected on Y1237, where both $n_a(T)$ and $n_b(T)$ display d-wave-like T dependencies.[9,33] Moreover, the direct observation of a PE-induced SC gap analogous to that seen in Y124 (Ref. 32) is not reported for Y1237. To explain this surprising difference between the two materials, a possibility is that the chain states in Y1237 are non-SC and the SC anisotropy is intrinsic to the planes. On the other hand, a d-wave behavior for each of $n_a(T)$ and $n_b(T)$ is consistent with calculations that consider *intrinsically* SC chains coupled to the planes by a Josephson-type pair tunneling.[10] If the latter is true, the d-wave T dependence of λ_b in Y1237 implies that there is a node in the SC gap on the chain FS. Both new ARPES experiments and detailed calculations can shed light on these proposals.

For $\mu_0 H > 2$ T, the $\mu_0 H$ dependence of the low-T VL properties in Y124 and Y1237 (Refs. 9 and 16) is more comparable, and indicates the two compounds display high-field SC regimes that become more similar. In both materials, γ_{ab} is always >1 which, to a first approximation, shows the persistence of the in-plane SC anisotropy to high field. Whether this anisotropy reflects a persistent contribution due to SC chain states, an intrinsic CuO_2 plane anisotropy, or is even related to the Fermi surface reconstruction in these materials,[34–36] remains an important open question.

Finally, we comment on an implication of our study concerning the interplay between coexisting SC and charge-density-wave (CDW) orders observed in a range of underdoped Y123 samples.[37–40] The CDW and SC orders compete since when applying a magnetic field to suppress superconductivity, the CDW order is observed to grow.[38] In Y124, no CDW order has yet been observed at zero field. Nevertheless, underdoped Y123 and Y124 both display comparable quantum oscillation frequencies,[34–36] and negative values of the Hall coefficient at low T.[41,42] This indicates similar $\mu_0 H$-driven reconstructions of the Fermi surface to occur in both Y123 and Y124, and which all likely involve CDW order. We speculate that the effect on the VL due to $\mu_0 H$-induced CDW order in Y124 may be similar to that due to $\mu_0 H$-induced spin-density-wave (SDW) order in $La_{2-x}Sr_xCuO_4$, $x = 0.145$.[43] There it was reported that the slope of the $\mu_0 H$-dependent VL form factor increases sharply at the onset of SDW order, after which the form factor falls with $\mu_0 H$ more rapidly than describable using conventional models.[26,44] The increase in slope was explained as caused by a disordering of the VL, which evidences the competition between the SC and SDW orders.[43] Since in Fig. 4(a) we observe no sharp change in slope of the form factor beyond that more easily understood in terms of a quenching of the PE, our results appear to limit any $\mu_0 H$-induced CDW order in Y124 to fields >6 T.

V. SUMMARY

In summary, we have studied the VL in $YBa_2Cu_4O_8$ (Y124) with $\mu_0 H \parallel \mathbf{c}$. At all fields, the VL structure is distorted due to the in-plane SC anisotropy. The VL distortion is suppressed with increasing $\mu_0 H$ which most likely reflects a quenching of a proximity-effect-induced SC gap involving chain states. Our results rule out a common framework for the low-field in-plane SC response of Y124 and $YBa_2Cu_3O_7$, and also indicate any $\mu_0 H$-induced CDW order in Y124 exists only for $\mu_0 H > 6$ T.

ACKNOWLEDGMENTS

We acknowledge discussions with J. Chang, A. T. Holmes, M. Ichioka, and K. Machida. SANS experiments were performed at the ILL, Grenoble, France, and the Swiss spallation neutron source, SINQ, PSI, Switzerland. We acknowledge financial support from the EPSRC of the UK, the University of Birmingham, the Swiss NCCR and its program MaNEP, and from the European Commission under the 6th Framework Programme though the Key Action: Strengthening the European Research Area, Research Infrastructures, Contract No. RII3-CT-2003-505925.

APPENDIX: TEMPERATURE-DEPENDENT FORM FACTOR AT $\mu_0 H = 0.4$ T

Here, we describe the analysis of T-dependent VL form factor data measured at $\mu_0 H = 0.4$ T. Unlike the data recorded at $\mu_0 H = 0.25$ T where the T dependence of both $|F(\mathbf{q}\,\text{vert}, T)|$ and $|F(\mathbf{q}\,\text{horiz}, T)|$ form factors was measured, at $\mu_0 H = 0.4$ T we only recorded the former. The T-dependent $|F(\mathbf{q}\,\text{vert}, T)|$ data measured at $\mu_0 H = 0.4$ T are shown in Fig. 6(a).

Next, we determine the T dependence of $n_b(T)$ at 0.4 T from the data shown in Fig. 6(a). We follow the same approach used when analyzing the $\mu_0 H = 0.25$ T data (Sec. III B 2), where we solve Eq. (2) at each T to find $\lambda_b(T)[\propto 1/\sqrt{n_b(T)}]$. In this instance, the calculation of $\lambda_a(T)$ is done using the values $\lambda_a(0) = 290$ nm, $\Delta_0(0) = 24$ meV determined from the fit of the $|F(\mathbf{q}\,\text{horiz}, T)|$ data shown in Fig. 5(b). For the zero-T coherence lengths, we again assume that $\xi_a(0) = 3.7$ nm and $\xi_b(0) = 3.6$ nm as reported in Sec. III B 1. The extracted T dependence of $n_b(T)$ at $\mu_0 H = 0.4$ T is shown in Fig. 6(b). Similarly, as seen at $\mu_0 H = 0.25$ T, $n_b(T)$ at 0.4 T displays a positive curvature in the low-T region which is incompatible with a simple d-wave superconducting (SC) gap function.

Using both the extracted T dependence of $n_b(T)$ and the assumed form of $n_a(T)$, in Fig. 6(c) we plot the T dependence of the anisotropy parameter γ_{ab}. For comparison, we also show

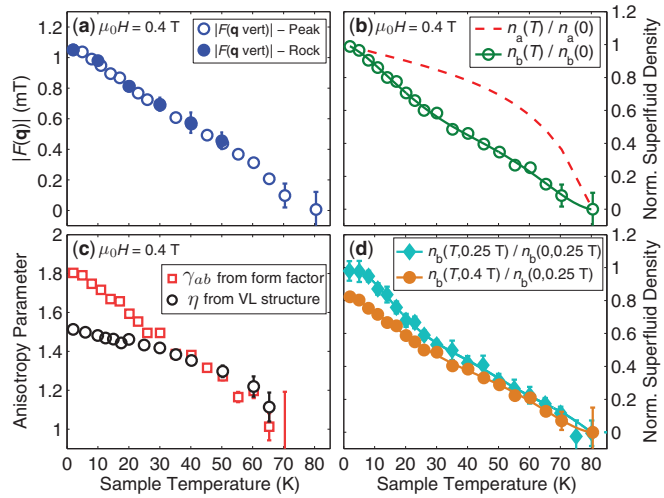

FIG. 6. (Color online) (a) A warming T dependence at $\mu_0 H = 0.4$ T of the $|F(\mathbf{q}\,\text{vert}, T)|$ VL form factors. Filled and empty symbols, respectively, denote measurements of full rocking curves, and measurements done just at the rocking-curve peak. (b) Normalized superfluid densities along **a** $[n_a(T)]$ and **b** $[n_b(T)]$. The dashed line is the ideal curve for $n_a(T)$ obtained from the fit presented in Fig. 5(b) of the main paper. The circles are values of $n_b(T)$ extracted as explained in the text, and the solid line is a guide to the eye. (c) The T dependencies at $\mu_0 H = 0.4$ T of γ_{ab} determined from the analysis of the T-dependent form factor, and η determined from T-dependent measurements of the VL structure. (d) The T dependence of $n_b(T)$ extracted at both $\mu_0 H = 0.25$ T and $\mu_0 H = 0.4$ T. The data at $\mu_0 H = 0.4$ T have been normalized using the extrapolated zero-T value of $n_b(0)$ at $\mu_0 H = 0.25$ T.

the T dependence of η determined from direct measurements of the T-dependent VL structure. Again, similarly as seen at $\mu_0 H = 0.25$ T, a clear disagreement between γ_{ab} and η emerges for $T \lesssim 30$ K, thus marking the irreversibility T at this field. The values of γ_{ab} at low T are thus larger than would be deduced solely by equating $\gamma_{ab} = \eta$ as expected in the local London approximation, although comparatively smaller than at $\mu_0 H = 0.25$ T. This reflects the $\mu_0 H$-induced suppression of $n_b(T)$, which is shown in Fig. 6(d). Here, we make a relative comparison between the $n_b(T)$ curves extracted at both $\mu_0 H = 0.25$ and 0.4 T. For making this comparison, both curves are normalized to the extrapolated value of $n_b(0)$ at $\mu_0 H = 0.25$ T. This shows clearly how $n_b(T)$ is suppressed with $\mu_0 H$, which we expect to reflect mostly a suppression of the proximity-effect-induced SC response involving chain electron states.

*jonathan.white@psi.ch

[1] W. A. Atkinson and J. P. Carbotte, Phys. Rev. B **52**, 10601 (1995).

[2] V. Z. Kresin and S. A. Wolf, Phys. Rev. B **46**, 6458 (1992).

[3] D. N. Basov, R. Liang, D. A. Bonn, W. N. Hardy, B. Dabrowski, M. Quijada, D. B. Tanner, J. P. Rice, D. M. Ginsberg, and T. Timusk, Phys. Rev. Lett. **74**, 598 (1995).

[4] J. L. Tallon, C. Bernhard, U. Binninger, A. Hofer, G. V. M. Williams, E. J. Ansaldo, J. I. Budnick, and C. Niedermayer, Phys. Rev. Lett. **74**, 1008 (1995).

[5] R. Daou, J. Chang, D. Leboeuf, O. Cyr-Choinire, F. Lalibert, N. Doiron-Leyraud, B. Ramshaw, R. Liang, D. A. Bonn, W. Hardy, and L. Taillefer, Nature (London) **463**, 519 (2010).

[6] D. H. Lu, D. L. Feng, N. P. Armitage, K. M. Shen, A. Damascelli, C. Kim, F. Ronning, Z.-X. Shen, D. A. Bonn, R. Liang, W. N.

Hardy, A. I. Rykov, and S. Tajima, Phys. Rev. Lett. **86**, 4370 (2001).

[7]D. A. Bonn, S. Kamal, A. Bonakdarpour, R. Ruixing, W. N. Hardy, C. C. Homes, D. N. Basov, and T. Timusk, Czech. J. Phys. **46**, 3195 (1996).

[8]A. Carrington, R. W. Giannetta, J. T. Kim, and J. Giapintzakis, Phys. Rev. B **59**, R14173 (1999).

[9]J. S. White, R. W. Heslop, A. T. Holmes, E. M. Forgan, V. Hinkov, N. Egetenmeyer, J. L. Gavilano, M. Laver, C. D. Dewhurst, R. Cubitt, and A. Erb, Phys. Rev. B **84**, 104519 (2011).

[10]T. Xiang and J. M. Wheatley, Phys. Rev. Lett. **76**, 134 (1996).

[11]R. Khasanov, A. Shengelaya, J. Karpinski, A. Bussmann-Holder, H. Keller, and K. Mller, J. Supercond. Nov. Magn. **21**, 81 (2008).

[12]A. Serafin, J. D. Fletcher, S. Adachi, N. E. Hussey, and A. Carrington, Phys. Rev. B **82**, 140506(R) (2010).

[13]S. T. Johnson, E. M. Forgan, S. H. Lloyd, C. M. Aegerter, S. L. Lee, R. Cubitt, P. G. Kealey, C. Ager, S. Tajima, A. Rykov, and D. McK. Paul, Phys. Rev. Lett. **82**, 2792 (1999).

[14]S. P. Brown, D. Charalambous, E. C. Jones, E. M. Forgan, P. G. Kealey, A. Erb, and J. Kohlbrecher, Phys. Rev. Lett. **92**, 067004 (2004).

[15]J. S. White, S. P. Brown, E. M. Forgan, M. Laver, C. J. Bowell, R. J. Lycett, D. Charalambous, V. Hinkov, A. Erb, and J. Kohlbrecher, Phys. Rev. B **78**, 174513 (2008).

[16]J. S. White, V. Hinkov, R. W. Heslop, R. J. Lycett, E. M. Forgan, C. Bowell, S. Strässle, A. B. Abrahamsen, M. Laver, C. D. Dewhurst, J. Kohlbrecher, J. L. Gavilano, J. Mesot, B. Keimer, and A. Erb, Phys. Rev. Lett. **102**, 097001 (2009).

[17]J. Karpinski, G. I. Meijer, H. Schwer, R. Molinski, E. Kopnin, K. Conder, M. Angst, J. Jun, S. Kazakov, A. Wisniewski, R. Puzniak, J. Hofer, V. Alyoshin, and A. Sin, Supercond. Sci. Technol. **12**, R153 (1999).

[18]V. G. Kogan, Phys. Rev. B **24**, 1572 (1981).

[19]L. J. Campbell, M. M. Doria, and V. G. Kogan, Phys. Rev. B **38**, 2439 (1988).

[20]S. L. Thiemann, Z. Radović, and V. G. Kogan, Phys. Rev. B **39**, 11406 (1989).

[21]V. G. Kogan, M. Bullock, B. Harmon, P. Miranović, L. Dobrosavljević-Grujić, P. L. Gammel, and D. J. Bishop, Phys. Rev. B **55**, R8693 (1997).

[22]M. Franz, I. Affleck, and M. H. S. Amin, Phys. Rev. Lett. **79**, 1555 (1997).

[23]M. Ichioka, A. Hasegawa, and K. Machida, Phys. Rev. B **59**, 8902 (1999).

[24]N. Nakai, P. Miranović, M. Ichioka, and K. Machida, Phys. Rev. Lett. **89**, 237004 (2002).

[25]D. K. Christen, F. Tasset, S. Spooner, and H. A. Mook, Phys. Rev. B **15**, 4506 (1977).

[26]A. Yaouanc, P. Dalmas de Réotier, and E. H. Brandt, Phys. Rev. B **55**, 11107 (1997).

[27]M. R. Eskildsen, Front. Phys. **6**, 398 (2011).

[28]J. Chang, N. Doiron-Leyraud, O. Cyr-Choinire, G. Grissonnanche, F. Lalibert, E. Hassinger, J.-P. Reid, R. Daou, S. Pyon, T. Takayama, H. Takagi, and L. Taillefer, Nat. Phys. **8**, 751 (2012).

[29]B. J. Ramshaw, J. Day, B. Vignolle, D. LeBoeuf, P. Dosanjh, C. Proust, L. Taillefer, R. Liang, W. N. Hardy, and D. A. Bonn, Phys. Rev. B **86**, 174501 (2012).

[30]The simplified band structure neglects an explicit SC chain band, but we expect $\lambda_a(T)$ to be insensitive to any superfluid density associated with the CuO chain states. This assumption is not necessarily true for the T variation of $\xi_b(T)$. However, at such a low applied field the exponential term in Eq. (2) that is dependent on $\xi_b(T)$ remains close to 1 (within ∼4%), and so the T-dependent behavior of $|F(\mathbf{q}\ \text{horiz})|$ is dominated by $\lambda_a(T)$.

[31]J. Sok, M. Xu, W. Chen, B. J. Suh, J. Gohng, D. K. Finnemore, M. J. Kramer, L. A. Schwartzkopf, and B. Dabrowski, Phys. Rev. B **51**, 6035 (1995).

[32]T. Kondo, R. Khasanov, J. Karpinski, S. M. Kazakov, N. D. Zhigadlo, Z. Bukowski, M. Shi, A. Bendounan, Y. Sassa, J. Chang, S. Pailhés, J. Mesot, J. Schmalian, H. Keller, and A. Kaminski, Phys. Rev. Lett. **105**, 267003 (2010).

[33] We note also that the effects of chain disorder, which can suppress a positive curvature in $n_i(T)$ (Ref. 45), are negated by studies on both Y124 and Y1237 which each have filled chains.

[34]N. Doiron-Leyraud, C. Proust, D. LeBoeuf, J. Levallois, J.-B. Bonnemaison, R. Liang, D. A. Bonn, W. N. Hardy, and L. Taillefer, Nature (London) **447**, 565 (2007).

[35]E. A. Yelland, J. Singleton, C. H. Mielke, N. Harrison, F. F. Balakirev, B. Dabrowski, and J. R. Cooper, Phys. Rev. Lett. **100**, 047003 (2008).

[36]A. F. Bangura, J. D. Fletcher, A. Carrington, J. Levallois, M. Nardone, B. Vignolle, P. J. Heard, N. Doiron-Leyraud, D. LeBoeuf, L. Taillefer, S. Adachi, C. Proust, and N. E. Hussey, Phys. Rev. Lett. **100**, 047004 (2008).

[37]G. Ghiringhelli, M. Le Tacon, M. Minola, S. Blanco-Canosa, C. Mazzoli, N. B. Brookes, G. M. De Luca, A. Frano, D. G. Hawthorn, F. He, T. Loew, M. M. Sala, D. C. Peets, M. Salluzzo, E. Schierle, R. Sutarto, G. A. Sawatzky, E. Weschke, B. Keimer, and L. Braicovich, Science **337**, 821 (2012).

[38]J. Chang, E. Blackburn, A. T. Holmes, N. B. Christensen, J. Larsen, J. Mesot, R. Liang, D. A. Bonn, W. N. Hardy, A. Watenphul, M. v. Zimmermann, E. M. Forgan, and S. M. Hayden, Nat. Phys. **8**, 871 (2012).

[39]A. J. Achkar, R. Sutarto, X. Mao, F. He, A. Frano, S. Blanco-Canosa, M. Le Tacon, G. Ghiringhelli, L. Braicovich, M. Minola, M. Moretti Sala, C. Mazzoli, R. Liang, D. A. Bonn, W. N. Hardy, B. Keimer, G. A. Sawatzky, and D. G. Hawthorn, Phys. Rev. Lett. **109**, 167001 (2012).

[40]T. Wu, H. Mayaffre, S. Krämer, M. Horvatić, C. Berthier, W. N. Hardy, R. Liang, D. A. Bonn, and M.-H. Julien,, Nature (London) **477**, 191 (2011).

[41]D. LeBoeuf, N. Doiron-Leyraud, J. Levallois, R. Daou, J.-B. Bonnemaison, N. E. Hussey, L. Balicas, B. J. Ramshaw, R. Liang, D. A. Bonn, W. Hardy, S. Adachi, C. Proust, and L. Taillefer, Nature (London) **450**, 533 (2007).

[42]P. M. C. Rourke, A. F. Bangura, C. Proust, J. Levallois, N. Doiron-Leyraud, D. LeBoeuf, L. Taillefer, S. Adachi, M. L. Sutherland, and N. E. Hussey, Phys. Rev. B **82**, 020514 (2010).

[43]J. Chang, J. S. White, M. Laver, C. J. Bowell, S. P. Brown, A. T. Holmes, L. Maechler, S. Strässle, R. Gilardi, S. Gerber, T. Kurosawa, N. Momono, M. Oda, M. Ido, O. J. Lipscombe, S. M. Hayden, C. D. Dewhurst, R. Vavrin, J. Gavilano, J. Kohlbrecher, E. M. Forgan, and J. Mesot, Phys. Rev. B **85**, 134520 (2012).

[44]J. R. Clem, J. Low Temp. Phys. **18**, 427 (1975).

[45]W. A. Atkinson, Phys. Rev. B **59**, 3377 (1999).